I R A M P
6(2), Dec. 2015, pp. 83-90

ISSN: 2229-3159

Laser-induced Plasma Tomography of Electron Density and Temperature

GHANESHWAR GAUTAM AND CHRISTIAN G. PARIGGER*

The University of Tennessee / UT Space Institute, Center for Laser Applications,
411 B.H. Goethert Parkway, Tullahoma, TN 37388-9700, USA
E-mail: cparigge@tennessee.edu

ABSTRACT: A Nd:YAG laser device is operated at the fundamental wavelength of 1064 nm to generate a micro-plasma in a hydrogen-nigtrogen gas mixture. The ultra-high-pure H_2 and N_2 ratio is 9 to 1 at a pressure of $1.21 \pm 0.03 \times 10^5$ Pa inside a chamber. Plasma emission spectra are recorded using a Czerny-Turner type spectrometer and an intensified charge coupled device. The line-of-sight measurements are Abel inverted to determine the spatial electron density and temperature distributions. The plasma kernel expansion speed is 2 km/s at a time delay of 100 ns and then decreases to 0.6km/s at 400 ns. The micro plasma dynamics that is initiated by focusing 140 mJ, 14 ns pulses can be modeled as an isentropic expansion for the investigated time delay range of 100 to 400 ns.

PACS Codes: 33.70.Jg, 32.70.Jz, 52.38.Mf, 52.50 Jm

Key Words: Laser-Induced Breakdown Spectroscopy, Line shapes and widths, Gases, Abel inversion, Tomography

1. INTRODUCTION

For the characterization of plasma, knowledge of species temperature and density is required. In this work, the determination of electron temperature and density is discussed to investigate the expansion dynamics after plasma generation with 14 ns pulsed Nd:YAG radiation. The work is motivated in part by a recent book on high-power laser-induced phenomena [1] and in part by numerous applications of laser-plasma for ablation and associated diagnostics in laser-induced breakdown spectroscopy.

The radiation from the plasma is typically recorded in a line-of-sight arrangement using time-resolved spectroscopy. Of interest in this work are the evaluation of the electron density, N_e, and temperature, T_e, using hydrogen Balmer series lines. For spherically symmetric plasma, the radial distribution of the plasma can be determined by laterally recording line-of-sight data and then by applying the Abel inversion. The Stark-broadened hydrogen Balmer series lines are studied for the purpose of constructing N_e and T_e 3-dimensional maps. For asymmetric plasma, data would need to be recorded by changing measurement angles with subsequent application of computer tomography based on Radon inversion techniques [2-4]. The Balmer series lines have been explored in various theoretical and experimental investigations and have been tested previously for the evaluation of the plasma parameters [5-9].

2. ELECTRON DENSITY AND TEMPERATURE

The electron densities during the early plasma decay can be determined using the hydrogen alpha line [10],

$$N_e[m^{-3}] = \left[\frac{\Delta\lambda[nm]}{1.31}\right]^{1.56} \times 10^{17}, \tag{1}$$

where the full width at half maximum, $\Delta\lambda$, is extracted from the Lorentz profile fitted data.

The Boltzmann plot method [11] is utilized for the measurement of electron excitation temperature. The integral values of H_α and H_β along with parameters that describe the optical transition are used. The temperature can be determined by finding the slope of the straight line,

$$\ln\left[\frac{I_{ki}\lambda_{ik}}{g_k A_{ki}}\right] = -\left[\frac{E_{ki}}{k_B T}\right] + \ln C. \tag{2}$$

For the constants in Equation (2), the following values are utilized [12]: Transition probabilities, $A_{ki} = 0.4410 \times 10^8$ s^{-1} and 0.08419×10^8 s^{-1}, statistical weights, $g_k = 18$ and 32, for the H_α and H_β lines, respectively. The central wavelengths of the transitions are indicated by λ_{ki}, the integrated line intensities are denoted by I_{ki}, E_{ki} are the energy differences of the transitions and k_B is the Boltzmann constant.An alternate approach for the determination of the electron temperature could be based on the line-to-continuum ratio of the hydrogen alpha and other Balmer series lines [4-6].

In view of hydrodynamic results [1], both electron density and temperature satisfy

$$\frac{T_e}{N_e^{2/3}} = \text{constant} \tag{3}$$

for isentropic expansion. This particular relation has been used previously in the description of laser-induced hydrogen plasma expansion [13]. However, these line-of-sight experiments employed a linear diode array for the determination of average density and temparature values. In this work, with the aid of an intensified 2-d arrray detector coupled to a spectrometer, data sets are recorded that allow one to perform integral inversions to extract spatial infromation of the plasma expansion.

The integratedline shapes of the H_α and H_β linescan be utilized to estimate the line ratios as function of temperature in the range of 10,000 to 100,000 K. In addition, results of detailed, recent Stark broadening calculations [7] can be used to determine N_e and T_e from the hydrogen Balmer series lines. Usually, normalized profiles are communicated as function of the reduced wavelength [5,6]. For constant $N_e = 1 \times 10^{17}$ cm^{-3}, the tabulated profiles [5] vary only slightly with temperature. However, in the spectral windows of the experiment (24 nm), the integrated values for H_α, H_β and H_γ acount for only 91%, 85% and 71%, respectively, of the total line profile.

Starting from the Boltzman plot Equation (2), the ratios of integrated profiles H_β/H_α, H_γ/H_α, H_δ/H_α and H_γ/H_β can be determined. Figure 1 illustrates the results.

Particularly the H_β/H_α line ratio is well suited for the determination of temperature in the 10,000 to 50,000 K range. Experimental errors appear to increase with diminished change of the ratio for higher temperature. In Figure 1, the horizontal line indicated the ratio in the limit of large temperature, $T_e >> 10$ eV.

The electron temperature can be determined from the recorded $H_{\acute{a}}$ and $H_{\grave{a}}$ lines. One would find the integral of the H_α and H_β lines, take the $H_{\hat{a}}/H_{\acute{a}}$ ratio,include the correction factors due to the spectral window used in the experiments and infer the temperature using Fig. 1(a). For instance, a ratio of 0.21 or 0.31 would imply a temperature of 10,000 and 20,000 K, respectively, for local thermodynamic equilibrium. However, for electron densities larger than 7×10^{17} cm^{-3}[24], the H_β lineis rather broad and possibly only the peak-separation can be utilized to estimate electron density. For that reason, the isentropic expansion relation in Equation (3) is investigated to infer the average temperature from line-of-sight data when only the H_α line is measured.

Diagnostics of laser-induced plasma at standard ambient temperature and pressure in laboratory air and hydrogen gas indicated close to spherically symmetric plasma kernels [14-17]. Here, optically thin and almost spherically symmetric laser produced micro-plasma is analyzed by applying the Abel inversion [18,19]. The radial intensity distribution, I(r,ë), of spherically symmetric plasma is connected by the Abel transform [14],

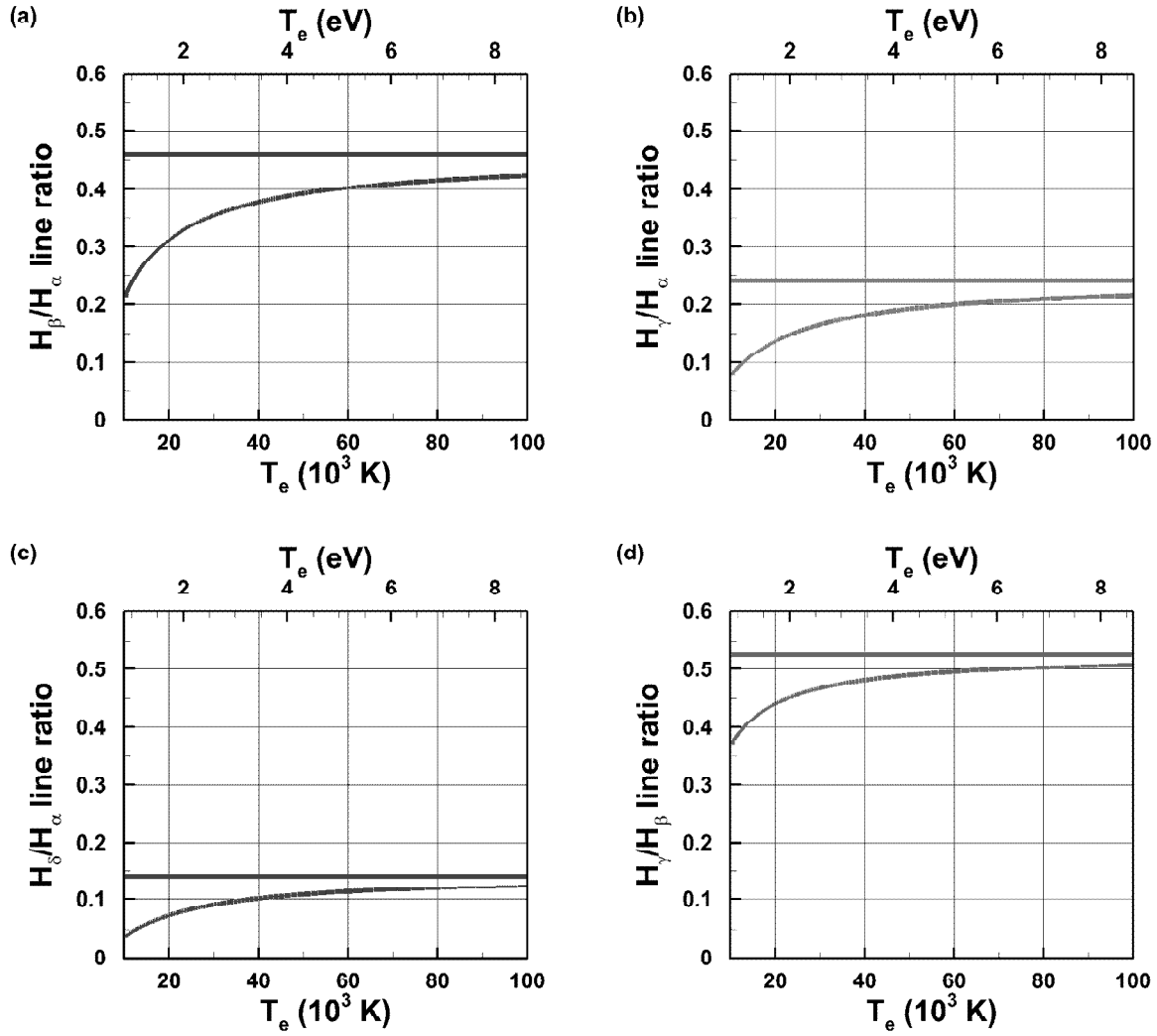

Figure 1: Computed integrated line ratios. (a) H_β/H_α, (b) H_γ/H_α, (c) H_δ/H_α and (d) H_γ/H_β

$$I(z,\lambda) = 2\int_z^\rho I(r,\lambda)\frac{r}{\sqrt{r^2 - z^2}}dr. \tag{4}$$

to the recorded wavelength-dependent lateral intensity distribution, I(z, λ). The variable z denotes the perpendicular distance from the origin to the line-of-sight, r is the radial distance from the center of the active plasma, and the upper integration limit is taken to be much larger, ρ >> R, than the radius, R, of the plasma that is modeled to be spherically symmetric. The spatial distribution is expected to show a spherical ring structure with lower electron density in the center of the expanding plasma [20], and accordingly, with lower electron temperature as expected from the isentropic expansion indicated in Equation (3). The slight deviations from spherical symmetry are also explored in this work.

Figure 2, shows the geometry for the Abel inversion of laterally collected line-of-sight spectra for an individual slice of micro-plasma. In the experiment, the laser beam is focused from the y-axis, i.e., into the page.

The spatial distribution is determined from the Abel inversions for each wavelength [14]. Slight asymmetries present in the recorded data is preserved by enumerating the symmetrized profile and introducing an asymmetric factor [14], subsequently, the asymmetric radial distribution can be determined. The asymmetry of the emitted radiation intensity may be due to laser pulse profile variation or due to the laser-plasma interaction that typically

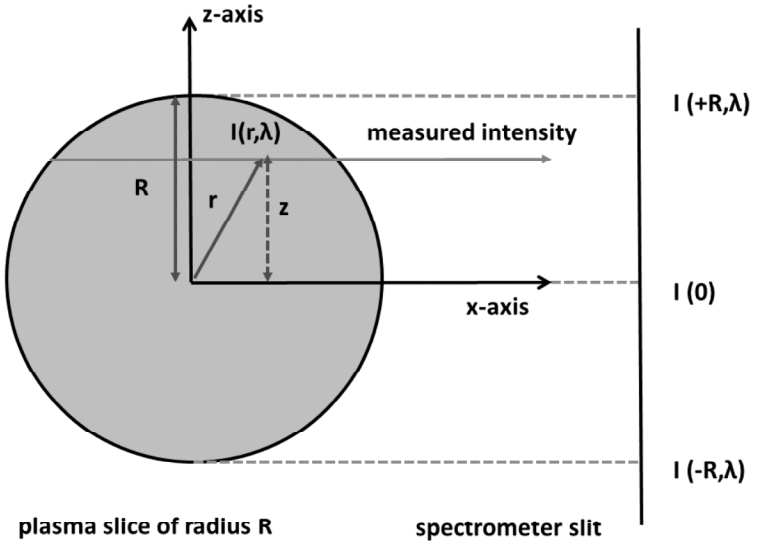

Figure 2: Schematic of the line-of-sight measurement of lateral data that are Abel inverted

occurs in nanosecond laser-induced plasma. The computed asymmetric and symmetric distributions for the electron density and temperature are consistent within the experimental error bars. In the analysis of the data discussed here, the recorded data are filtered by using Savitzky-Golay filter before employing the Abel inversion algorithm.

3. EXPERIMENTALDETAILS

In the experimental arrangement as shown in Figure 3, ultra-high-pure (UHP) hydrogen and nitrogen gases are filled inside a cell at a ratio of 9 to 1. Micro-plasma is generated by using a Nd:YAG laser device (Quanta Ray model DCR-2(10)) that is operated at the fundamental wavelength of 1064 nm to generatethe 14 ns pulses. The laser beam is directed perpendicular to the slit height and focused with f#/5 optics.

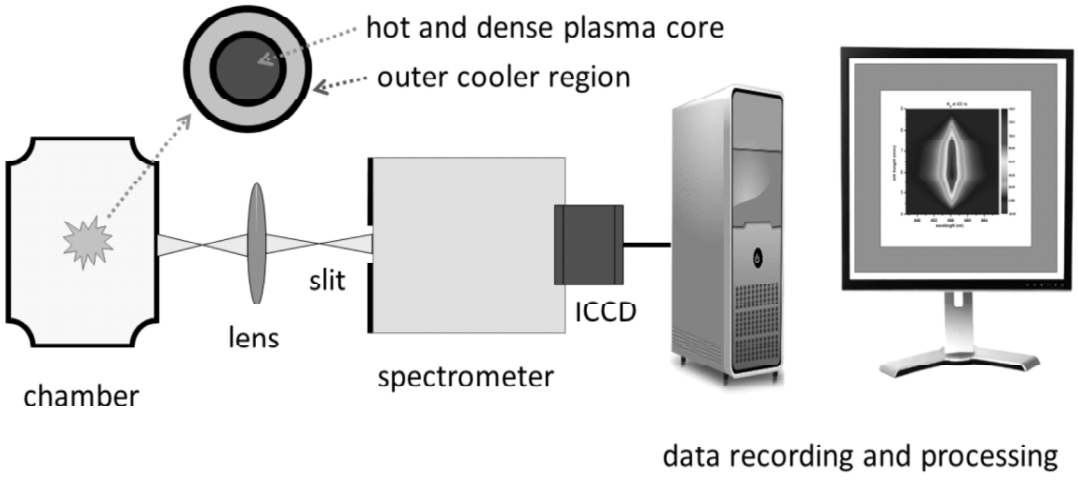

Figure 3: Experimental schematic of plasma generation and measurement of spectra

A 1200 grooves/mm holographic grating is used to disperse the plasma emission. Spatial and temporal information of the plasma spectra are recorded using a Czerny-Turner type spectrometer and an intensified charge-coupled device (ICCD). The ICCD consists of a 1024 × 1024 pixel array with 1024 horizontal pixels for wavelength and 1024 vertical pixels for intensities. Each pixel corresponds to 13.6 μm, therefore each lateral measurement has a resolution of 13.6 μm with the 1:1 imaging accomplished by the lens indicated in the schematic.

4. RESULTS

Figure 4, displays wavelength calibrated and detector's sensitivity corrected plasma spectra. These images represents the map of emission intensity as a function of slit height and wavelength. Lateral information of the emission intensity along the slit height is subjected to Abel inversion to determine the spatial distribution of the recorded, wavelength dependent data. For the Abel inversion process, 73 spectra at the slit heights from 0.60 mm to 1.59 mm are analyzed.

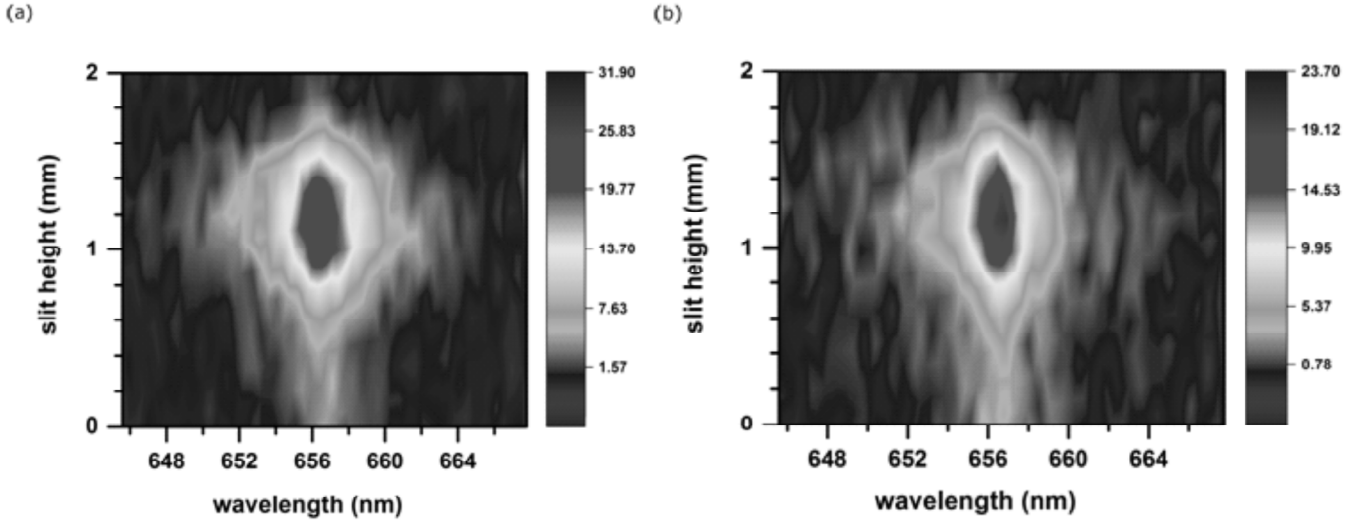

Figure 4: H_α spectra from 9 to 1 H_2 and N_2gas mixture. Time delay (a) 200 ns, (b) 300 ns. The contourplot scalingis from minimumto maximum

Figure 5, depicts the symmetrical radial distributions of the electron densities obtained from $H_á$ line profiles. Recorded experimental data points are first Abel inverted and then Lorentz fitted before using the empirical formula given in Equation (1) to evaluate the electron densities. The results for electron densities indicate a major ring structure near the radius of ± 0.2 mm. In pure hydrogen and for identical Nd:YAG laser parameters and ambient pressure, the major ring structure is near ± 0.5 mm at a time delay of 400 ns [14]. For $N_e \geq 20 \times 10^{17}$ cm^{-3} (~0.1 amagat), the self-absorption effects for $H_á$appear to be noticeable in UHP hydrogen and laboratory air plasma [21]. This would imply that the electron density values at 100 ns may be over-predicted by a factor of 1.5 when comparing with H_β.

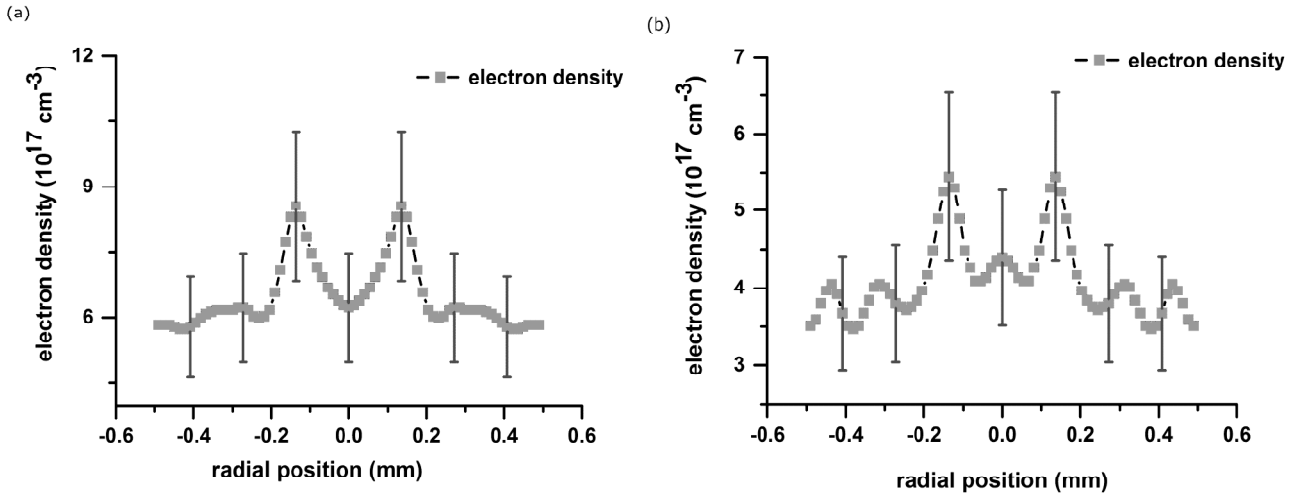

Figure 5: Symmetric distributions from H_α widths. Time delay (a) 200 ns, (b) 300 ns. The vertical error bars indicate the experimental error margins

Following the procedure for slight asymmetric, spherical expansion [14], the deviations in the prediction of the electron-density profiles are within the estimated ± 20% error bars. Figure 6 displays the corresponding slightly asymmetric, Abel-inverted results for the electron density.

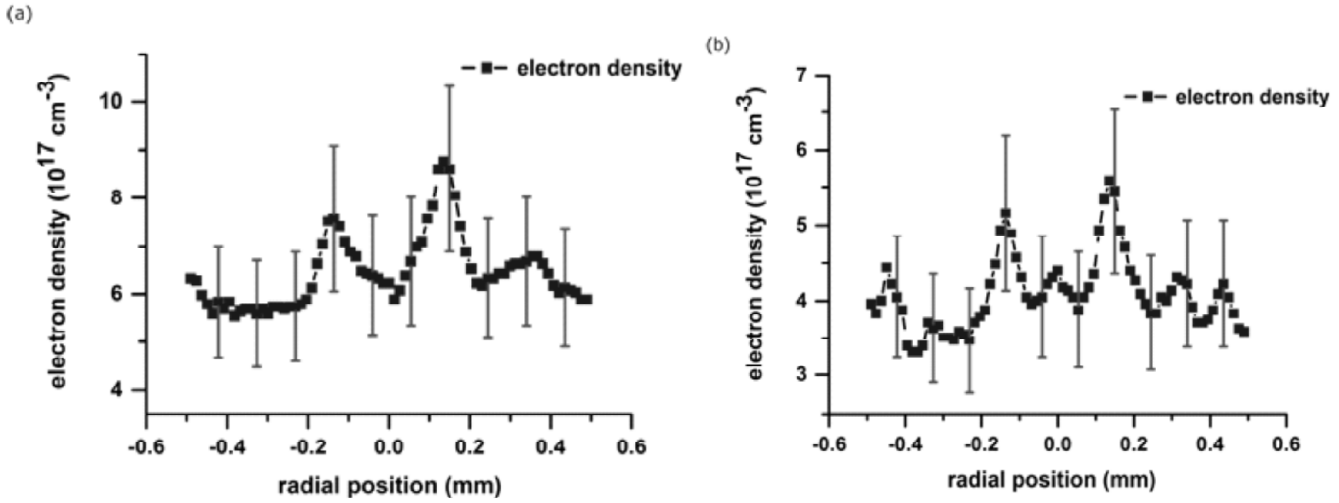

Figure 6: Asymmetric distributions from H_{α} widths. Time delay (a) 200 ns, (b) 300 ns. The asymmetric vs. symmetric results indicate agreement within experimental error bars

The radial temperature distributions are deduced from Boltzmann plots usingH_{α} and H_{β} lines. Figure 7 illustratesthe results. The plasma kernel expansion speeds amounts to 2.3 ± 0.5 km/s and 1.3 ± 0.3 km/s at the time delays of 100 ns and 200 ns. Equally, kernel expansion speeds of 1.0 ± 0.2 km/s and 0.6 ± 0.1 km/s are predicted for the time delays of 300 ns and 400 ns.

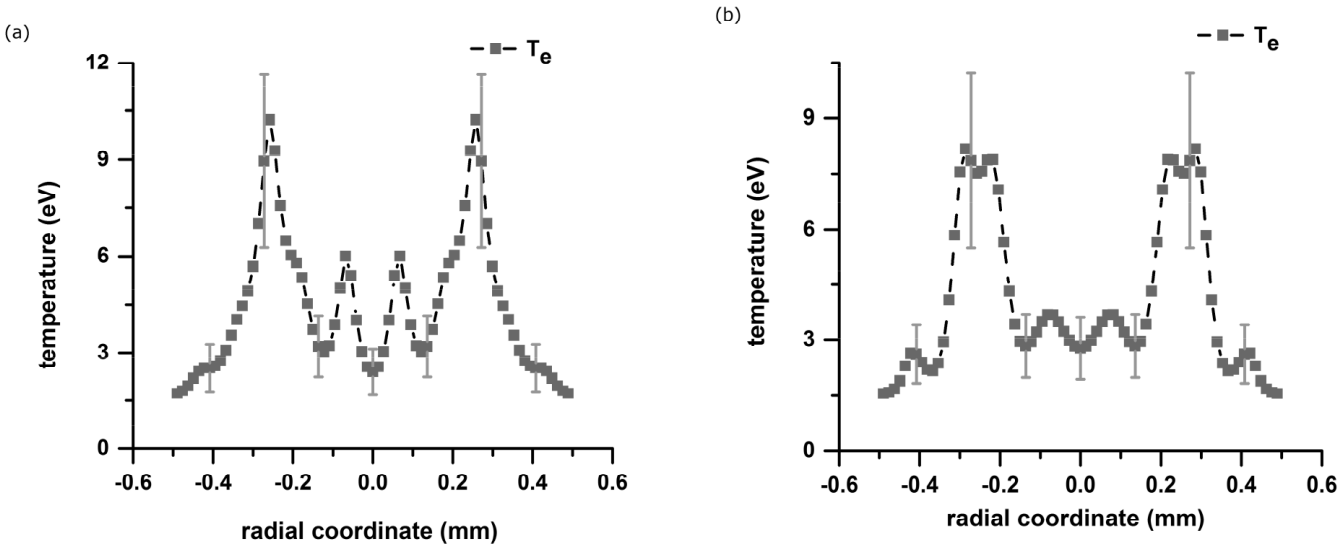

Figure 7: Symmetric temperature distributions. Time delay (a) 200 ns, (b) 300 ns. The 30% error bars are primarily due to uncertainties in the integrated H_{α} and H_{β} line intensities

Minor peaks are discernible in Figure 7 near the center and are due to the expanding kernel. In comparison, simulations of Cu vapor plume expansions with He gas background predict a low gas density near the target and a high density in front of the vapor plume including the formation of a shock front [22]. For the 300 ns time delay measurements, the temperatures are of the order of 3 eV in the center, the peaksshow at least 2 × higher $T_e$due to the kernel expansion. It is noteworthy, that Thomson scattering diagnosticsin the study of laser ablation in ambient air

[23] reveal electron temperature of 61×10^3 K (5.3 eV) in the central region but for a time delay of 600 ns from the laser ablation pulse, diminishing to 13×10^3 K (1.1 eV) at a time delay of 3 μs from optical breakdown. Therefore, the determined electron temperatures indicated in Fig. 7 appear in reasonable agreement with the Thomson scattering laser ablation experiments. The determined temperature values at 400 ns are consistent within the error margins of recently communicated hydrogen laser-induced plasma experiments [15].

The average values of electron densities are 16, 6.5, 4.1 and 3.2×10^{17} cm^{-3} at the time delays of 100, 200, 300 and 400 ns, respectively. Likewise, the average temperature values are 55, 51, 47 and 38×10^3 K (4.8, 4.4, 4.0 and 3.3 eV) at 100, 200, 300 and 400 ns, respectively. For standard temperature and slightly above atmospherics pressure (1.21×10^5 Pa), the electron density of 3.2×10^{17} $cm^{-3}$is expected to be a factor of 1.9 higherfor the 9:1 gaseous hydrogen:nitrogen mixture than for the pure gaseous hydrogen experiments [20,24] at a pressure of 1.08×10^5 Pa. Using the isentropic expansion (Eq. (3)) a factor of 1.9 higher N_e implies lower temperature by a factor of 1.5 ($1.9^{2/3}$). In other words, a temperature of 38×10^3 K at a time delay of 400 ns determined in the 9:1 hydrogen:nitrogen mixture experiment is consistent with 57×10^3 K obtained in the pure hydrogen experiment for a time delay for 450 ns [24].

For an isentropic expansion of the electron distribution in laser-induced plasma dynamics [1,13], the ratio of the electron temperature and electron density to the power of 2/3 is expected to be constant, see Equation (3). Table 1 shows the results determined from the average values of electron density and temperature.

Table 1
$N_e^{2/3}$and T_e ratiosfor the time delay range of 100 to 400 ns

$(N_{e,100} / N_{e,200})^{2/3}$	1.37± 0.13	$T_{e,100} / T_{e,200}$	1.08± 0.32
$(N_{e,200} / N_{e,300})^{2/3}$	1.36 ± 0.09	$T_{e,200} / T_{e,300}$	1.09± 0.33
$(N_{e,300} / N_{e,400})^{2/3}$	1.17 ± 0.08	$T_{e,300} / T_{e,400}$	1.22 ± 0.37

The ratios in Table 1 imply that the electronic component of the plasma is well-characterized by an isentropic expansion as previously discussed for pure hydrogen laser-induced plasma. The average electron density $N_{e,100}$ appearsover-predicted from H_α spectra by a factor of 1.5 [15,21] due toself-absorption effects.A ratio $(N_{e,100} / N_{e,200})^{2/3} = 1.82$ would be outside the error margins; however, the value of $(N_{e,100} / N_{e,200})^{2/3} = 1.37$ is obtained when including a correction factor of 1.5 to lower $N_{e,100}$, thereby effectively accounting for self-absorption. The results for the $(N_{e,300} / N_{e,400})^{2/3}$ and $T_{e,300} / T_{e,400}$ ratios are affected by lower signal to noise data than for the other ratios, but again, the results support the isentropic expansion within the error margins.

5. CONCLUSIONS

The radial electron density and temperature distributions of the 9 to 1 hydrogen to nitrogen atmospheric mixture and for the time delays of 100 to 400 ns showspherical shell structures. For these time delays, the temperature in the central region of the plasma is cooler than in the expanding spherical shell.The kernel expansion speed is close to the speed of sound in hydrogen gas. The time resolved spectroscopy experiments together with the Abelinversion of laterally recorded data reveal high peak temperatures.

Acknowledgments

The authors greatly appreciate support in part for this work by the Center for Laser Applications at The University of Tennessee Space Institute.

References

[1] P. Mulser, D. Bauer, *High Power Laser-Matter Interaction*, Springer, Berlin, (2010).

[2] S. Eschlbçck-Fuchs, A. Demidov, I. Gornushkin, T. Schmid, R. Rçssler, N. Huber, U. Panne, J. Pedarnig, *Spectrochim. Acta Part B***123** (2016) 59.

[3] H.-J. Kunze, *Introduction to plasma spectroscopy*, Springer, Berlin, (2009).

[4] J. Cooper, Rep. Prog. Phys. **29** (1966) 35.

[5] H. R. Griem, *Plasma Spectroscopy*, McGraw-Hill, New York (1964).

[6] H. R. Griem, *Spectral Line Broadening by Plasmas,* Academic Press , New York, (1974).

[7] E. Oks, *Stark Broadening of Hydrogen and Hydrogenlike Spectral Lines in Plasmas*, *The Physical Insight*, Alpha Science(2006).

[8] C. G. Parigger, *Spectrochim.Acta B***79-80** (2013) 4.

[9] N. Konjeviæ, M. Ivkoviæ, N. Sakan, *Spectrochim. Acta Part B***76**(2012) 16.

[10] D. M. Surmick, C. G. Parigger, *Int. Rev. At. Mol. Phys.***5(2)**, (2014) 73.

[11] W. L. Wiese, *Spectrochim. Acta Part B* **46** (1991) 831.

[12] W. L. Wiese and J. R. Fuhr, *J. Phys. Ref. Data* **38** (2009) 565.

[13] C. G. Parigger, J. W. L. Lewis, D. Plemmons, *J. Quant. Spectrosc. Radiat. Transfer* **53** (1995) 249.

[14] C. G. Parigger, G. Gautam, D. M. Surmick, *Int. Rev. At. Mol. Phys.* **6** (2015) 43.

[15] C. G. Parigger, D. M. Surmick, G. Gautam, Self-absorption characteristics of measured laser-induced plasma lines, *J. Phys.: Conf. Ser.* (in press, 2016).

[16] M. Thiyagarajan, J. E. Scharer, *IEEE Trans. Plasma Sci.***36** (2008) 2512.

[17] H. Sobral, M. Villagrán-Muniz, R. Navarro-González, A. C. Raga, *Appl. Phys. Lett.* **77**, (2000) 3158.

[18] G. Pretzler, *Z. Naturforsch*, **46a** (1991) 639.

[19] C.Killer, *http://www.mathworks.com/matlabcentral/fileexchange/43639-abel-inversion-algorithm*, "Abel Inversion Algorithm," (last accessedFebruary 15, 2016).

[20] G. Gautam, C. G. Parigger, Electron density and temperature diagnostics in laser induced hydrogen plasma, *J. Phys.: Conf. Ser.* (in press, 2016).

[21] C. G. Parigger, L. Swafford, D. M. Surmick, M. Witte, A. Woods, G. Gautam, *J. Phys.: Conf. Ser.*, **548**, (2014) 012043.

[22] A. Bogaerts, M. Aghaei, D. Autrique, H. Lindner, Z. Y. Chen, W. Wendelen, *Adv. Mat. Res.***227.1**, (*Trans. Tech. Publ., 2011*).

[23] A. Mendys, M. Kañski, Farah-Sougueh, S. Pellerin, B. Pokrzywka, K. Dzier¿)ga, *Spectrochim. Acta Part B***96**, (2014) 61.

[24] C.G. Parigger, D.H. Plemmons, E. Oks, *Appl. Opt.* **42** (2003) 5992.